

# Impact Crater Detection on Mars Digital Elevation and Image Model

Mert Degirmenci  
Middle East Technical University,  
Turkey  
mert.degirmenci@ceng.metu.edu.tr

Shatlyk Ashyralyev  
Middle East Technical University,  
Turkey  
shatlyk.ashyralyev@ceng.metu.edu.tr

## ABSTRACT

As outer space image acquisition techniques progress, larger amounts of planetary data sets become available. Impact crater statistics about planets is an important resource as use of this information reveals geological history. Since manual detection of impact craters requires substantial human resource, there is a compelling need to investigate automated crater detection algorithms. In this study, we develop a novel framework to detect Martian impact craters by fusing data obtained from Mars Global Surveyor. In our proposed method, extracted craters from Mars Digital Image Model (MDIM) are crosschecked by using Mars Digital Elevation Model (MDEM). Multi population genetic algorithm (MPGA) has been devised to extract craters from scale invariant feature set found by SIFT algorithm. In order to decrease the number of false positives, extracted from MDIM are validated by detected basins from MDEM. Experimental results on NASA databases suggest high crater detection rates.

## 1 INTRODUCTION

Impact craters are formed by collision of two celestial bodies. Planetary science utilizes the impact crater databases to extract characteristic information about both colliding bodies. Reliably extracted crater features enable geologists inspect hydrological processes, and climatic information about the planet under consideration. Surface age prediction also relies on size and frequency distributions of craters. Quest for geological information about recently scanned planets stimulates the need for impact crater databases. Impact crater detectors are also utilized in space exploration. Spacecrafts need to incorporate a crater detector for visual positioning. In order to land on asteroids autonomously, spacecrafts must calculate the locations of the impact craters based on 3D model of the space and 2D images obtained. Both usage area of a crater detector system requires highly accurate results.

In order to create credible crater databases, a number of scientists have manually examined the optical satellite images and gathered information about crater features. The most comprehensive data set, known as Barlow catalog, includes characteristic information for more than 40,000 craters on Mars [Bar88]. Even though visual inspection of satellite images may reveal key information about impact craters, this process eventually becomes infeasible upon arrival of large volume sensor data. Recently acquired sensor data have increased the number of research studies about automatic impact crater detection.

Significant number of researchers has used optical images to detect impact craters. These visibility based methods have limitations with regard to illumination, surface characteristics, and occlusion. Although most impact craters have obvious circular features, impact angle and geological deformations severely affect visibility of them. Significant overlap between craters also degrades accuracy of automatic crater detectors using optical sensor data captured at frequently hit areas of the planets. To address these challenges, we propose a data fusion approach for

impact crater detection. Our algorithm reduces the error by fusing elevation data and optical data. In this section, we address previously researched optical image-based and elevation-based crater detection algorithms.

Existing body of research on crater detection algorithms generally focus on optical images to produce scalable crater databases. Most of the proposed frameworks incorporate either unsupervised or supervised methods to identify features and whereabouts of impact craters. Unsupervised techniques focus on finding rims and merging them to locate the crater. Hough transform based methods are generally incorporated in this class of techniques. Supervised learning methods, on the other hand, involve kernel-based and neural network based learning methods for training. Support Vector Machines are usually used as classifiers in crater detection.

Since high level of accuracy is needed for a crater database to be utilized by planetary scientists, researchers have combined several crater detection algorithms in order to produce more accurate results. Sawabe et al. have used multiple boundary based approaches and merged the results obtained [Saw06]. In the first approach they have used images that are classified considering illumination. When shady and illuminated pattern is recognized, they fit a circle to the surrounding edges. Although abrupt brightness changes may reveal a lot about the surface under consideration, the presence of sensor data with correct illumination is often an unrealistic assumption to make. The second approach they have used tries to find edge pixels of interest using a vectorized feature extractor proposed by Sugiyama et al. [Sug97]. Then a roundness measure is checked for identification of circles. Other two approaches proposed by Sawabe et al. uses Hilditch's thinning algorithm and fuzzy Hough transform in addition to previously discussed algorithms respectively.

All of the described approaches proposed by Sawabe et al. up to now suffer from elliptic shape of impact craters. Depending on geological deformations on the sur-

face, there is a high possibility that craters form degraded ellipses rather than circles on the surface. In fact, most craters in the Barlow catalog can hardly be characterized by circularity features [Bar88].

Machine learning approaches have also been applied in order to detect and catalog impact craters. Wetzler et al. have used various supervised learning algorithms, including ensemble methods (bagging and AdaBoost with feed-forward neural networks as base learners), support vector machines (SVM), and continuously scalable template models (CSTM) to derive crater detectors from ground-truthed images [Wet05]. They have noted that the SVM solution to the problem performs superior on crater detection and localization compared to boundary-based approaches such as Hough Transform [Wet05]. However, their implementation demands huge ground-truth data and computational resource considering that SVM models they found involved approximately five thousand support vectors. In order to overcome large computational demands, they have proposed using blocked-FFT implementation of the SVM decision function [Bur04].

A number of researchers have used combination of supervised and unsupervised techniques to detect impact craters. Kim et al. propose three staged crater detection system [Kim05]. In the first stage, they eliminate noise in the image by extracting region of interest. They also consider edge direction, and illumination angle at this stage. In the second stage of their algorithm, which they call organization stage, primitive arcs are organized by graph and conic section fitting. Candidate craters are propagated to the last stage, where they are verified by a fitness measure and a false crater classifier based on artificial neural networks.

Honda et al. have also combined machine learning approaches with boundary based methods [Hon00]. In the framework they have proposed, image is first binarized. To find craters, circular object detection is then applied using a combination of Hough Transform and Genetic Algorithm. At the last stage, they have utilized Self-Organizing Maps to categorize candidate craters. The two frameworks discussed above incorporate both supervised learning techniques and boundary based analysis of optical satellite imagery.

Ellipse fitting algorithms are frequently used when researchers model the crater to be detected as an ellipse. Clustering techniques such as K-means are generally used for partitioning the feature points into set of candidate craters. Leroy et al. have employed the same idea to isolate individual craters [Ler01]. After partitioning, they have fit an ellipse on the boundary of the craters. Although boundary based methods provide simple yet powerful crater detectors, they noted that illumination angle and noisy sensor data may obstruct detecting impact craters. In order to alleviate these problems, researchers have complicated the focusing process of crater detection by smoothing and applying morphological operations to optical images. Marchetti et al. notes that smoothing image increases robustness to

noise significantly [Mar04]. However, the information contained in optical data for overlapping craters may be lost due to smoothed image.

Recently, NASA revealed sufficiently precise and comprehensive digital image (DIM), and elevation (DEM) data on Mars. This advancement lead to more reliable crater extractors. Researchers have used raw DEM data to detect impact craters. Bue et al. have discussed limitations of optical image data and outlined an algorithm using solely digital elevation model [Bue07]. They utilized elevation of the surface to detect basins. Idea of Bue's study was to merge high curvature edges and basins of elevation model to detect crater rims. Located crater rims are passed through a set of morphological operations to thin and close the gaps. They applied Hough Transform to detect craters and noted significant improvements over optical image based crater detectors. Their findings are important to us since this was the first study using DEM to detect impact craters. Improvements can be promised over their implementation by incorporating digital image data. Machine learning approaches can also be included to increase the accuracy of their craters detector.

In this study, we address inherent challenges in crater detection such as limitations of image acquisition techniques and deformations of craters. We improve the accuracy of existing crater detectors by fusing the results obtained from height data and optical image data. Next section gives an overview of the framework proposed.

## 2 OVERVIEW

Our framework can be decomposed into two modules. These are ellipse detection and basin detection modules. The two result set obtained are merged at the end to increase the reliability of the algorithm. In this section, algorithms involved in both components of the system are described. Following sections include more detailed discussion of the methods.

Optical image processing module first computes scale invariant feature transform of the image proposed by Lowe [Low99]. Main reason we have used SIFT features is their robustness to scale, orientation, and affine distortion. Scale invariance is especially important considering high scale variance between craters to be detected on Mars. These features fed into a multi population genetic algorithm to find ellipses. Detected ellipses are verified by results of DEM processing module.

Elevation data processing module smoothes the height map of the Mars surface. Smoothing the surface increases the accuracy of the basin extraction process. The basins are found using drainage network extraction algorithm proposed by Freeman et al. [Fre92]. Sink sources of the height map are generally craters to be detected. However, Martian landscape involves non-crater basins as well. Thus, basin detection module of the framework is generally not enough to be used as a reliable crater extractor. This is the reason we fuse the results obtained of basin and crater detection modules. The flowchart of the system is given in Figure (1).

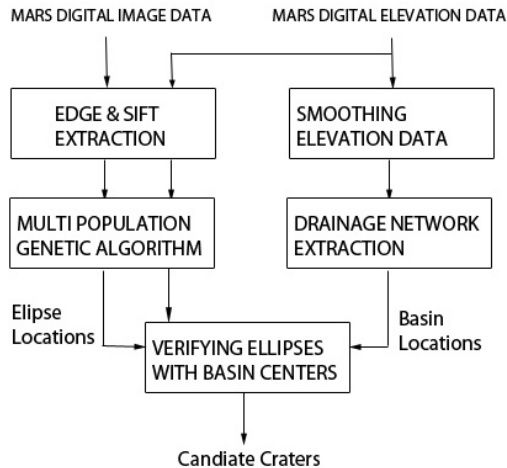


Figure 1: Overview of crater detector system

### 3 CRATER EXTRACTION FROM DIM

As described in the overview section of this document, we employ scale invariant feature transform and multi population genetic algorithm to find impact craters from optical data. In this section, we will give a detailed description of both algorithms involved.

#### 3.1 Scale Invariant Feature Transform

Although the existing body of research on impact crater detection focus on extracted edges, we have also implemented SIFT algorithm which aims to reliably identify scale invariant features of an object proposed by Lowe [Low99]. Compared to the edges extracted, SIFT features are well localized around the rims of the craters as seen in Figure (2). The method that Lowe has proposed transforms image into collection of feature vectors that are invariant to scaling, rotation, and illumination changes. SIFT algorithm involves four main stages, which are scale-space extrema detection, keypoint localization, orientation assignment, and keypoint descriptor. Keypoints are defined as the extrema points of Difference of Gaussians (DoG) that occur at multiple scales. The reason of using DoG instead of gaussians is to gain efficiency. The algorithm eliminates outliers by discarding low-contrast keypoints and edge responses.

SIFT features have gained popularity in computer vision domain due to its successful applications in feature matching. Recently, SURF (Speeded Up Robust Features), a faster version of the SIFT algorithm has been proposed which is based on Haar Wavelet responses [Bay08]. Although SURF feature detector is faster than SIFT, a comparative study between SURF and SIFT reveals that SURF features are not stable against rotation and illumination changes [Jua09]. This is the main reason we have used SIFT features in our study of a crater detector. High rotation variation between craters and illumination changes are possible due to the Mars surface, image acquisition equipment used, and the camera parameters involved.

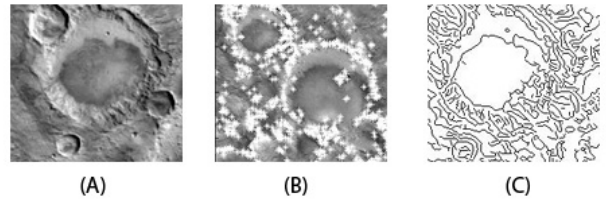


Figure 2: (A) Optical data obtained from Mars surface (B) SIFT features highlighted (C) Edges extracted by canny edge detector

#### 3.2 Genetic Algorithm Variants for Ellipse Detection

In our implementation of crater extractor from DIM, craters are assumed to have elliptic shape. Since SIFT features extracted from previous stage of our system are assumed to be scale invariant, elliptic assumption of the feature vector is reasonable.

Most methods to detect ellipses from images can be categorized into two major groups. These are Hough Transform (HT) based methods, and stochastic algorithms.

HT based methods perform a mapping from image space to parameter space. The optima's of parameters corresponds to instances of primitives. Although HT is highly accurate and feasible to use for primitives with small number of parameters, computational demands of the method grows exponentially along with the parameter number [Yin99]. Since we need to detect ellipses which have five arbitrary parameters, HT based methods are infeasible to use because of large parameter space involved.

Stochastic algorithms have also been applied for geometric primitive extraction on 2D images since primitive extraction has been shown to be an optimization problem [Rot93]. Most popular stochastic algorithm used for primitive extraction is genetic algorithm (GA). Inspired by evolutionary biology genetic algorithm tries to find an approximate solution to optimization problems. Instead of exhaustively searching parameter space as in the case of HT, GA iteratively refines population to cluster solutions around the global optima. Moreover, inherently parallel nature of GA can be exploited on parallel computing architectures to produce scalable algorithms. A number of researchers have already used this idea to cope with growing datasets [Deg10].

Although GA based techniques have inherent strengths over HT based methods, finding multiple instances of a geometric primitive can't be directly mapped into problem space of GA because it approximates a global maximum. However, in our crater detection implementation, we want to detect several locally maximum ellipses rather than finding the globally optimal ellipse in the image. This is the reason we have implemented a multi population genetic algorithm that is able to find several locally optimal ellipses in the given image.

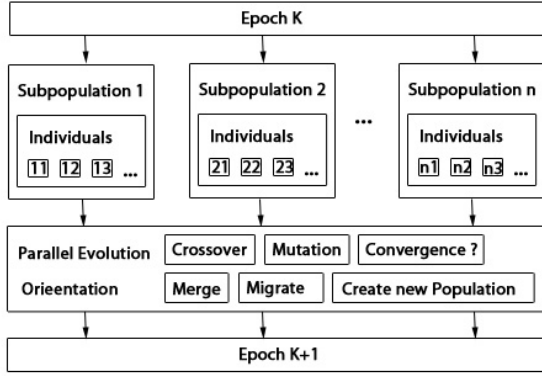


Figure 3: One iteration of Multi-Population Genetic Algorithm

The classical genetic algorithm implementation may also suffer from premature convergence. The term is used for harmfully fast convergence of a population to a suboptimal solution. The two commonly used solutions to this problem are fitness sharing and replacement of similar individuals. Both of the proposed modifications to genetic algorithm maintains the diversification of the population in order not to converge directly to a premature solution. The former, also called Sharing Genetic Algorithm (SGA), is proposed by Lutton et al. [Lut94]. SGA shares the fitness of similar individuals to decrease clustering around a single solution. The later, on the other hand, simply replaces the similar individuals with randomly generated ones to increase the diversity of the population. Although the replacement is necessary as the fittest individuals dominate the population, replacing with random individuals degrades the performance of the genetic algorithm since it may lead the population to an already searched space. Thus, SGA has inherent strengths over replacement of similar individuals method. Note that, SGA can also be used for the local optima search problem since it reduces the fitness values of individuals clustered around single optima.

The multi-population genetic algorithm (MPGA) is another variant of GA that can be used for multiple local optima detection. A number of subpopulations are generated and evolved in order to find several optima's. These subpopulations can be thought as islands where individuals can travel in between and create their own one. This adaptive clustering mechanism both concentrates the solutions around optimal points and diversifies the population across the search space. A research study conducted by Yao et al. investigates the use of both MPGA and SGA over the ellipse detection problem [Yao05]. Results of their study reveals that MPGA outperforms SGA in terms of both accuracy and performance. Following section of this document, describes the multi-population genetic algorithm used for ellipse detection on SIFT keypoints.

### 3.3 MPGA for Ellipse Detection

In the ellipse detection context, multi-population genetic algorithm evolves several populations aimed to represent

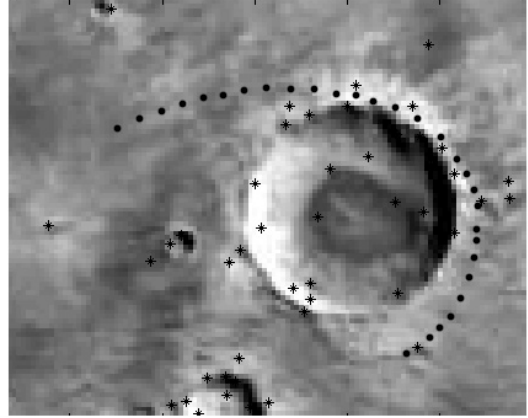


Figure 4: A chromosome that defines an ellipse over five keypoints

ellipses from keypoints extracted. Figure (3) shows one iteration of MPGA where a number of populations evolve in parallel. Communication between subpopulations are performed through migration of individuals from one subpopulation to another. Creation of a new population is also possible when an individual does not exhibit an affinity with any existing populations. As the number of epochs increase, subpopulations can possibly replicate each other which would decrease the performance. To prevent this danger, our MPGA algorithm considers the merging the similar subpopulations.

In the convergence case of a subpopulation, the keypoints of detected ellipse is removed from the image, and the individuals are deported. Note that, as the number of subpopulations decrease the number of individuals per population will increase. Thus, search will accelerate as the number of ellipses in the image decreases.

As seen in the Figure (3), MPGA can be characterized by a set of operations on individuals; crossover, mutation, fitness evaluation, and orientation. Orientation of an individual requires a set of operations for habitat selection, which are merging, migration, and new subpopulation generation. This section describes all stages of MPGA in the context of ellipse detection.

**Individual Representation** Individuals, also referred as chromosomes, are candidate ellipse parameters. As seen in Eq. (1), an ellipse can be represented with it's five arbitrary parameters.

$$p_0x^2 + 2p_1xy + p_2y^2 + 2p_3x + 2p_4y + 1 = 0 \quad (1)$$

where  $(x,y)$  denotes the  $x$  and  $y$  coordinates of the feature points, and  $p_{0..4}$  are parameters of the ellipse.

Given any five points  $(x_i, y_i)$  where  $i \in \mathbb{Z} : 0 \leq i \leq 4$ , parameters of an ellipse passing through them can be computed by solving five linear equations given in Eq. (2).

$$\begin{bmatrix} x_0^2 & 2x_0y_0 & y_0^2 & 2x_0 & 2y_0 \\ x_1^2 & 2x_1y_1 & y_1^2 & 2x_1 & 2y_1 \\ x_2^2 & 2x_2y_2 & y_2^2 & 2x_2 & 2y_2 \\ x_3^2 & 2x_3y_3 & y_3^2 & 2x_3 & 2y_3 \\ x_4^2 & 2x_4y_4 & y_4^2 & 2x_4 & 2y_4 \end{bmatrix} \begin{bmatrix} p_0 \\ p_1 \\ p_2 \\ p_3 \\ p_4 \end{bmatrix} = \vec{0} \quad (2)$$

Using this fact, the chromosome of an individual can be composed of five keypoints. In the literature, there are other individual representations for ellipse detection. Mainzer represents an individual directly by five parameters of the ellipse [Man02]. That is the parameters  $p_{0..4}$  are encoded in the chromosomes of population. However, as Yao et al. noted that this representation generates a larger search space since the solutions may not even represent an existing ellipse. In our implementation, on the other hand, search is focussed on existing ellipses since chromosomes encode real keypoints extracted from optical images of Mars. In our implementation minimal point representation have been used for chromosome encoding. Figure (4) depicts an individual chromosome that is represented by a dashed ellipse over five keypoints extracted. Blue stars on the image shows the keypoints extracted by SIFT algorithm.

**Fitness Evaluation** In order to evaluate how fit the individual is, genetic algorithm requires a fitness function that returns a comparable value given a chromosome. Ellipse detection algorithms that involve the GA have widely match template around the ellipse represented by an individual. Mainzer et al. suggests fitness function at Eq. (3) that punishes edge pixels far from the ellipse [Man02] for each pixel  $(x,y)$  on the candidate ellipse.

$$f_1 = \sum_{x,y} \max_{\forall i,j} [E(x+i,y+j) - \frac{1}{c}(|i|+|j|)] \quad (3)$$

$$\text{where } E(x,y) = \begin{cases} 1 & \text{if Image}(x,y) \text{ is an edge pixel} \\ 0 & \text{Otherwise} \end{cases}$$

Considering that this operation has to be performed whenever a fitness of an individual has to be calculated, efficiency should be optimized. Distance map data structure stores the closest distance to an edge for each pixel in the original image. An approximation to a distance map can be realized by a set of morphological operations.

The research studies that aim to extract ellipses from 2D images rely on detected edges [Yao05]. However, imagery data obtained from the surface of the Mars exhibits high illumination variances and outlier edges. Instead of using only edge responses for evaluating the fitness of an individual, the keypoints extracted by SIFT algorithm have also been utilized. The distance map for SIFT features and the edges have been computed using morphological dilation with structuring image as 4x4 normal distribution. The fitness is then calculated as given in Eq. (4) that matches an ellipse around the set of feature points.

$$f_2 = w_1 f_1 + w_2 \sum_{x,y} \max_{\forall i,j} [S(x+i,y+j) - \frac{1}{c}(|i|+|j|)] \quad (4)$$

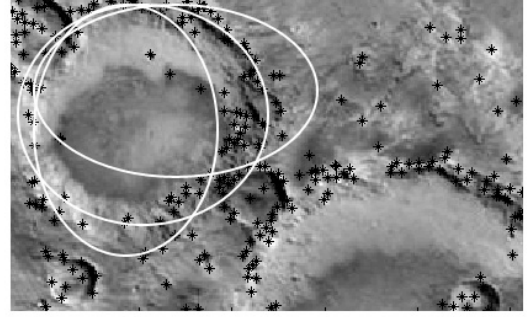


Figure 5: Uniform crossover operation over two individuals  $P_1$  and  $P_2$  which produces the offspring  $O_1$

where  $E(x,y)$  and  $f_1$  are as in Eq. (3),  $w_1$  and  $w_2$  are weights determining the importance of edge response and SIFT features respectively. The equation for  $S(x,y)$  is given in Eq. (5).

$$S(x,y) = \begin{cases} 1 & \text{if Image}(x,y) \text{ a SIFT keypoint} \\ 0 & \text{Otherwise} \end{cases} \quad (5)$$

**Merging of Subpopulations** As subpopulations evolve, converging ones may replicate in the population. In this case, all subpopulations evolve through a one globally optimal crater. To prevent replication, close subpopulations should be merged. Euclidean distance between cluster means can be used as closeness measure of two subpopulations. In literature, researchers have applied an empirical threshold over cluster distances to determine whether a merging operation should occur or not [Yao05]. However, scale variant distance measurements are not stable for small number of subpopulations. In our implementation, Mahalanobis distance is measured to check the merging condition.

While merge operations are begin performed, half of the fittest individuals are selected for a new subpopulation as suggested by Yao et al. [Yao05]. However, this implementation of merging operation causes the population to decrease. If a population undergo many merging operations, premature convergence problem may arise since the size would not be adequate to find all optima's. To prevent this side effect, size of each subpopulation is increased to compensate for the loss. The chromosomes of the introduced individuals are randomly generated from the set of keypoints.

**Migration & Splitting** On each evolution iteration of the population, chromosomes select the subpopulation with the least Mahalanobis distance. If a chromosome is not sufficiently close to any subpopulation, it creates a new subpopulation center of which is itself.

**Crossover** Uniform crossover has been implemented to produce offsprings. Since the individuals are represented by five feature points, the uniform crossover operation merely swaps the points of one parent with the other to produce an offspring. The offspring bears the subset of parents keypoints. Figure (5) shows the uniform crossover operation over two chromosomes.

**Mutation** The mutation operation is defined as randomly changing a gene of the chromosome and reassigning it to a new value. The operation is required to lead search towards uninhabitant areas. However changing one keypoint randomly generally results in degraded ellipse if the individual to be mutated is sufficiently fit. Therefore, mutation operation has to be enhanced to change more than one keypoints of the chromosome. In our implementation, a random number of keypoints have been replaced by mutated ones.

#### 4 BASIN EXTRACTION FROM DEM

When two celestial bodies collide, a basin is usually formed at the larger colliding body. The abrupt height variation on the surface of planets survive longer than the rims of the basins which are degraded due to erosional processes. The optical data obtained does not carry any information about the height of the surface. Therefore, elevation data obtained from Mars surface have been utilized to find the basin locations. Researchers have proposed several approaches to find sink sources in elevation data. Most of the algorithms developed can be classified as either hydrological or morphological approach. The former approach uses the flooding algorithm of a water to detect sink sources, while the later recognize basins by their shape.

Since the impact craters on the Mars surface form topographic basins, hydrological algorithms outperform on basin location extraction. The survey of sink point extractors shows that the algorithm proposed by Callagan et al. is being used commonly [Kis04]. In Callagan's algorithm a rain drop is assumed in each cell of the elevation model with eight possible flowing directions [Cal84]. Due to predetermined flow direction for each cell, the algorithm is also called "Deterministic 8" (D8). The cell that the rain drop will flow into is determined by the slope of the eight possible flow directions.

Although Callagan's algorithm provide simple and realistic flow simulation, the method fails on planar surfaces where surface runoffs are prevalent. To increase the reliability of the method, Freeman proposed multiple flow direction model that can find divergent flow drainage points by favoring water flow to several adjacent cells of lower elevation [Fre92]. The amount of water distributed from a higher elevation rain drop,  $d_i$ , is given in Eq. (6).

$$d_i = \frac{\max(0, S_i^w)}{\sum_{j=1}^8 \max(0, S_j^w)} \quad (6)$$

where  $S_j$  is the slope of adjacent cells, and  $w$  is a constant factor determining the divergence of the flow.

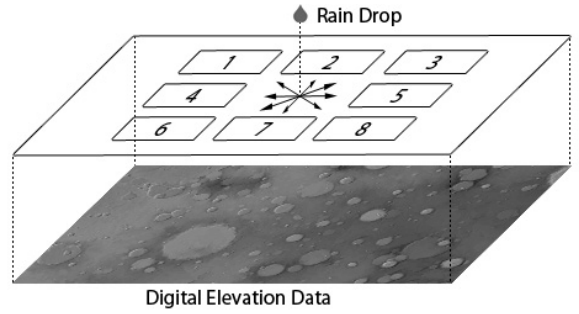


Figure 6: Sink source detection on Mars Digital Elevation Model

The distribution of the water drop is proportional to the slope of adjacent cells as Eq. (6) suggests. We have applied the multiple flow direction model to calculate the locations of the sink sources. Since the elevation data of the Mars surface is highly vibratile, the DEM data is first smoothed before the drainage networks are extracted. Figure (6) shows a rain drop with the flow directions on the Mars digital elevation data. Once the flow of water is stabilized, the resulting image of rain drop catchments is propagated to the last stage of our algorithm where the results of DEM and DIM data is fused.

#### 5 MERGING RESULTS

The framework proposed have operated on two data set with two different algorithms. The result set is composed of the most fit ellipses extracted from DIM & DEM data and the image of basin locations obtained from DEM data. The figure (7) shows the set of ellipses extracted from optical and elevation data. The complementary nature of the results increases the robustness of the algorithm. Note that a portion of the ellipses extracted do not correspond to the craters. To decrease number of false positives, the basins extracted should be used to verify the ellipses.

To finalize the decision about the existence of impact craters, for each ellipse the ratio of the ellipse area and the catchment area under the ellipse is calculated. This metric is thresholded with fixed constant determined by our empirical studies. Finally the fittest ellipses extracted from DEM & DIM data are merged to compose candidate craters. To eliminate duplicate ellipses, the overlapping area is compared with the area of the bigger ellipse for each pair of ellipses. If the duplication is detected, the result of DEM data is output since ellipses obtained from DEM data have shown higher accuracies.

#### 6 EXPERIMENTS & RESULTS

The test site we have selected for our experiments contains heavily cratered area that includes famous Herschel crater. The digital elevation and optical data is obtained from web map server (WMS) of NASA. Mars Digital Image Mosaic (MDIM) and Mars Orbital Laser Altimeter (MOLA) downloaded from WMS have the approximate bounding box as  $7.42^\circ, -18.42^\circ, 172.02^\circ, -7.58^\circ$ . The terrain chosen contains large number of degraded craters as well as non-crater

basins and other topographic structures. Another reason for choosing this area is the significant overlap over Barlow Catalog and the test sites previously chosen by researchers [Bue07].

The data retrieved from WMS is partitioned into 113 images of size 720x360 and overlapping ratio 1/4. The performance of the algorithm is measured by the metrics at Eq. (7-9). These metrics are proposed by Shufelt [Shu99] and have been used to measure the performance of crater detectors by a number of researchers [Bar04], [Kim05], [Bue07].

$$Detection = \frac{100TP}{TP + FN} \quad (7)$$

$$Branching = \frac{FP}{TP} \quad (8)$$

$$Quality = \frac{100TP}{TP + FP + FN} \quad (9)$$

In Eq. (7-9), TP, FP, and FN are abbreviations for True Positives, False Positives, and False Negatives respectively. The Detection metric measures the crater detection performance. The Branching metric measures the delineation performance. And Quality can be thought as measure of overall performance of the algorithm.

The researchers who have proposed crater detection algorithms have chosen different test sites. Some of them have even chosen test sites that do not include degraded craters [Kim05]. In order to test for reliability, we have selected a challenging terrain that includes highly degraded craters as in [Bue07]. The results are compared with both manually detected Barlow crater database and automatic crater detection algorithms proposed by researchers [Kim05], [Bue07], [Bar04]. The table 6 shows their findings. The D,B, and Q represents the metrics given in Eq. (7-9). Nontrivial test sites includes terrains where heavily degraded craters are common. The trivial test site used by Kim et al. includes only well-formed craters since they have noted that the algorithm is not capable of detecting the degraded craters [Kim05].

Our test site has more than 1/3 overlap with nontrivial test sites. The algorithm developed in this document had detected 621 craters in 113 segments. The number of non craters that were detected is 127. Thus, the Branching factor of our study is approximately 0.26. This is the lowest branching factor in the literature of impact crater detectors test on nontrivial test sites (see Table 6). Most false positives correspond to degraded rims of large impact craters with diameter > 20 km. The second best performing algorithm in terms of branching factor includes curvature profile calculation, basin detection, and hough transformation [Bue07]. Although Bue et al. have proposed a confirmation algorithm to verify the candidate craters found by Hough Transform, their verification strategy did not rely on separate set of calculations as in our case.

The algorithm we have proposed failed to detect 182 impact craters that are listed on Barlow Catalog. Most of the craters that our algorithm has failed to detect shows substantial deformations due to erosional processes. The de-

	D	B	Q	Test Site	Ref.
Bue	74%	0.29	61%	Nontrivial	[Bue07]
Barlow	75%	0.00	75%	Nontrivial	[Bar88]
Barata	64%	1.65	31%	Nontrivial	[Bar04]
Kim	88%	0.15	78%	Trivial	[Kim05]

Table 1: Detection, Branching, and Quality metrics for different crater-detection algorithms

tection rate is approximately 73% in our nontrivial test site. The rate of detection accomplished by this research is close to the best performing automatic crater detection algorithm in the literature [Bue07] and to the human detection rate [Bar88]. The overall quality metric of our algorithm is also approximately equal to the Bue’s study with 61%.

The comparisons in this section are made between similar test sites. The study of Kim et al. has not been compared to our study because of their simple test site selection. The metrics of the algorithm proposed in this document suggests higher quality when the test site is chosen not to include degraded craters.

## 7 CONCLUSION

This document describes an algorithm for Martian impact crater detection on Mars digital image and elevation data. Data fusion approach for the DEM and DIM is a contribution that improved the reliability of existing crater detectors. The use of Scale-Invariant Features and Multi-Population Genetic Algorithm is also novel for the literature of the crater detectors. The experimental results suggest a high detection rates close to the best performing algorithm and the most comprehensive crater catalog prepared manually. The improvements over the framework proposed are possible since the fitness evaluation procedure of MPGA can be complicated with other measures such as curvature profiles and heuristics. The adaptation of MPGA certainly introduces the flexibility that the current set of algorithms proposed lack. The complexity of fitness function can be traded with accuracy. It remains a future work for the authors to experiment with different fitness functions to optimize the performance of the algorithm. The aim of this study is to introduce a novel framework that is extensible and reliable to the literature of Hough Transform based algorithms.

## REFERENCES

- [Bar88] N. G. Barlow, Crater size-distributions and a revised Martian relative chronology, *Icarus*, vol. 75, pp. 285-305, 1988.
- [Kim05] J.R. Kim, J.P. Muller, S.V. Gasselt, J.G. Morley, G. Neukum, Automated Crater Detection, A New Tool for Mars Cartography and Chronology, *Photogrammetric Engineering and Remote Sensing*, vol. 71, No. 10, pp. 1205-1217, 2005.
- [Ler01] B. Leroy, G. Medioni, E. Johnson, L. Matthies, Crater detection for autonomous landing on asteroids,

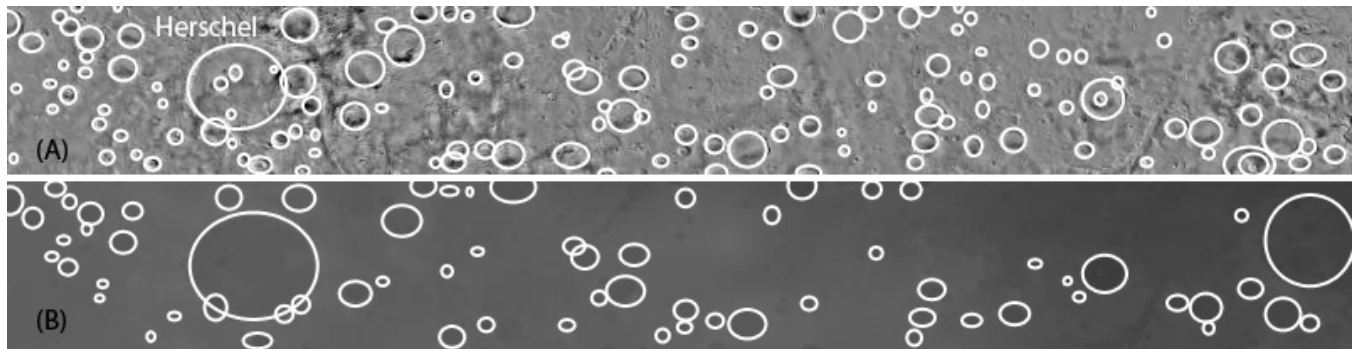


Figure 7: (A) The ellipses detected on Mars Digital Image Mosaic (B) The ellipses detected on Mars Orbital Laser Altimeter, both acquired on  $120.42^\circ$  West,  $-18.42^\circ$  South,  $172.00^\circ$  East,  $-10.58^\circ$  North.

- Image and Vision Computing, vol. 19, pp. 787-792, 2001.
- [Wet05] Wetzler, P. G., Honda, R., Enke, B., Merline, W. J., Chapman, C. R., and Burl, M. C., Learning to Detect Small Impact Craters, in Proc. of the Seventh IEEE Workshops on Application of Computer Vision, vol. 01, 2005.
- [Saw06] Y. Sawabe, T. Matsunaga, S. Rokugawa, Automated detection and classification of lunar craters using multiple approaches, *Advances in Space Research*, Volume 37, Issue 1, The Moon and Near-Earth Objects, pp. 21-27, 2006.
- [Sug97] Sugiyama, T., Abe, K., 1997. Edge feature analysis by a vectorized feature extractor and in multiple edge. *IEIC, D-2, J80-D-2, 6*, pp. 1379-1389, 1997.
- [Hon00] R. Honda, R. Azuma, Crater Extraction and Classification System for Lunar Images, technical report at Department of Mathematics, Kochi University, 2000.
- [Bur04] M.C. Burl, P.G.Wetzler, Resource-constrained Application of Support Vector Machines to Sensor Data, *Data Mining in Resource-Constrained Environments*, 2004.
- [Bue07] B. D. Bue, T. F. Stepinski Machine Detection of Martian Impact Craters From Digital Topography Data, *IEEE Trans. Geosci. and Remote Sens.*, vol.45, pp.265-274, 2007.
- [Mar04] B. L. Marchetti, L. Bruzzone, L. Lizzi, P. G. Marchetti, J. Earl, M. Milnes, Recognition And Detection Of Impact Craters From Eo Products, 2004.
- [Low99] D. G. Lowe, Object Detection from local scale-invariant features, *Proceedings of the International Conference on Computer Vision*, pp. 1150-1157, 1999.
- [Cal84] J. F. O'Callaghan, D. M. Mark, The extraction of drainage networks from digital elevation data, *Comput. Vis. Graph. Image Process.*, vol. 28, no. 3, pp. 328-344, Dec. 1984.
- [Bay08] H. Bay, A. Ess, T. Tuytelaars, L. V. Gool, SURF: Speeded Up Robust Features, *Computer Vision and Image Understanding (CVIU)*, Vol. 110, No. 3, pp. 346-359, 2008.
- [Jua09] L. Juan, O. Gwun, A Comparison of SIFT, PCA-SIFT and SURF, *International Journal of Image Processing (IJIP) Volume(3), Issue(4)* pp 143-152, 2009.
- [Yin99] P.Y. Yin, A new circle/ellipse detector using genetic algorithms, *Pattern Recognition Letters*, Volume 20, Pages 731-740, Issue 7, 1999.
- [Rot93] G. Roth and M. D. Levine, Extracting geometric primitives, *Comput. Vision. Graphics Image Processing: Image Understanding*, vol. 58, pp. 1-22, 1993.
- [Lut94] E. Lutton, P. Martinez, A genetic algorithm for the detection of 2D geometric primitives in images. *Proceedings of the 12th international conference on pattern recognition*, pp. 913, 1994.
- [Yao05] J. Yao, N. Kharma, P. Grogono, A multipopulation genetic algorithm for robust and fast ellipse detection, *Pattern Analysis & Applications*, vol. 8 pp. 149-162, 2005.
- [Deg10] M. Degirmenci, Complex geometric primitive extraction on graphics processing unit, *journal of WSCG, Winter School of Computer Graphics*, Volume 18, No.1-3, pp. 129-134, 2010.
- [Man02] T. Mainzer, Genetic algorithm for shape detection, Technical report no. DCSE/TR-2002 06, University of West Bohemia, 2002.
- [Fre92] T.G. Freeman, Calculating catchment area with divergent flow based on a regular grid, *Computer and Geoscience*, pp.413-422, 1991.
- [Kis04] R. Kiss, Determination of drainage network in digital elevation models, utilities and limitations, *Journal of Hungarian Geomathematics*, Volume 2, pp. 16-29, 2004.
- [Shu99] J. A. Shufelt, Performance evaluation and analysis of monocular building extraction from aerial imagery, *IEEE Trans. Pattern Anal. Mach. Intell.*, vol. 21, no. 4, pp. 3113-3126, 1999.
- [Bar04] T. Barata, E. Ivo Alves, J. Saraiva, and P. Pina, Automatic recognition of impact craters on the surface of mars, in Proc. ICIAR, Porto, Portugal, pp. 489-496, 2004.